Silicon Photonic Single-Sideband Generation with Dual-Parallel Mach-Zehnder Modulators

Ashok Kodigala, Michael Gehl, Christopher T. DeRose, Dana Hood, Andrew T. Pomerene, Christina M. Dallo, Douglas C. Trotter, Penny Moore, Andrew L. Starbuck, Jongmin Lee, Grant Biedermann, and Anthony L. Lentine
Applied Photonic Microsystems
Sandia National Laboratories
Albuquerque, NM 87123
akodiga@sandia.gov, mgehl@sandia.gov

***Abstract*— We demonstrate a silicon photonic single-sideband (SSB) modulator with dual-parallel Mach-Zehnder modulators (MZMs) operating at telecommunication wavelengths near 1550 nm. The modulator has a carrier suppression greater of 27 dB and at least 12 dB sideband suppression at 1 GHz with minimal optimization. This performance can be improved with further optimization.**

Keywords—optical single-sideband (OSSB) modulation; silicon photonics; mach-zehnder modulator (MZM)

I. Introduction

With the increased demand for silicon photonics over the last decade, there is a growing need for efficient single side-band (SSB) technologies on a silicon platform for frequency shifting or conversion with applications ranging from high-resolution spectroscopy to dense wavelength division multiplexed (D-WDM) networks [1-2]. However, to date, much of SSB work is heavily concentrated on a lithium niobate ($LiNbO_3$) platform [2-3]. The few SSB modulators realized on silicon often lack carrier suppression and/or employ resonant ring modulators [4]. Hence, they have lower efficiencies and are not readily suitable for high-power applications. Moreover, some of these SSB generation techniques requires the filtering of one sideband from a double-sideband (DSB) output via a frequency matched notch or band-reject filter thereby limiting the bandwidth [1].

II. Design

In what follows, we use a dual-parallel nested MZMs configuration to generate a SSB that cancels the unwanted sideband and simultaneously suppresses the carrier thus alleviating the need for output filters (see Figure 1) [2]. We have four carrier-depletion phase modulators (in orange) along with multiple thermos-optic (TO) phase shifters (in blue). The four modulators are split into two pairs of balanced modulators (top and bottom pair). The two balanced modulators are fed optically and electrically in quadrature. Within each arm of a pair, they are π out of phase both optically and electrically, which leads to carrier suppression. The relative phase shifts between the top and bottom pairs leads to suppression of one of the fundamental sidebands, *i.e.* unwanted sideband.

III. Experiment

Figure 2a shows the experimental setup to test our SSB modulator performance. We test the modulator with a 1 GHz RF signal. This signal is divided into four using three hybrid 3dB couplers (one 180˚ and two 90˚ couplers). The output spectra was measured with a scanning Fabry-Perot (FP)

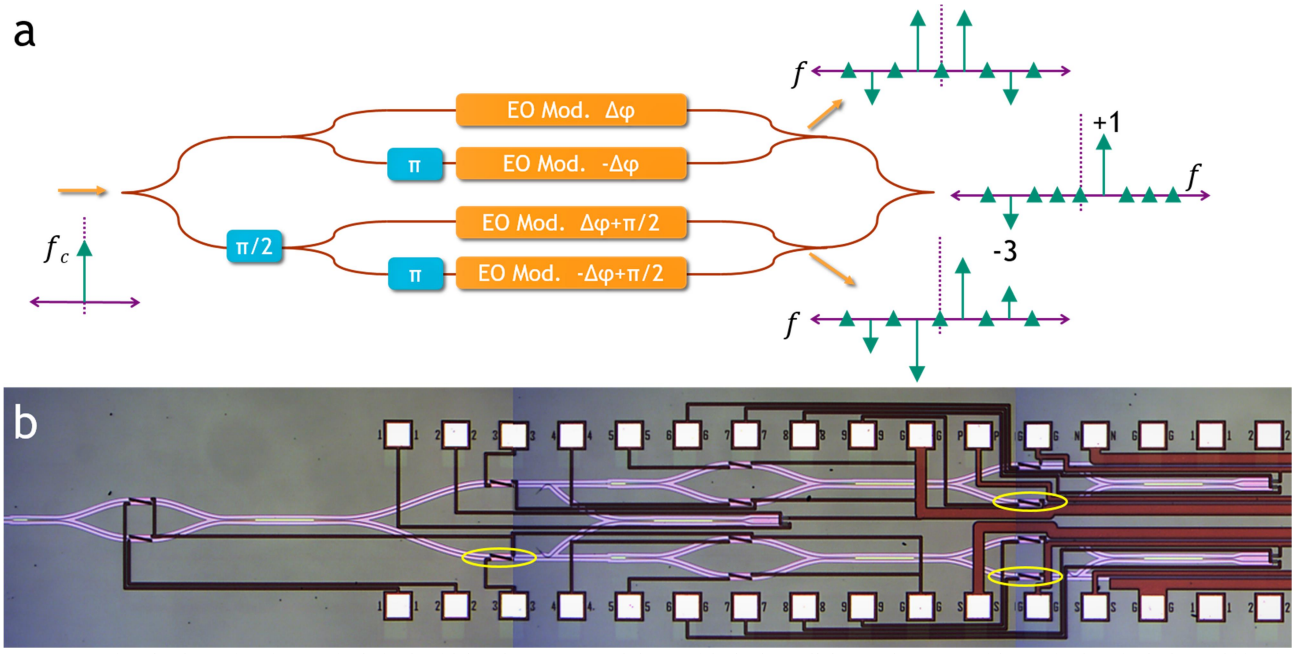

Fig. 1. (a) Operational schematic of an optical single-sideband (OSSB) modulator with dual-parallel nested MZMs with required optical phase shifts (in blue) and RF phase offsets (in orange). (b) Micrograph image of equivalent device under test with resistive heating elements (highlighted in yellow) serving as thermo-optic (TO) phase shifters followed by electro-optic (EO) phase modulators. Additional TO elements along with multimode interference (MMI) splitters for finer control are also pictured.

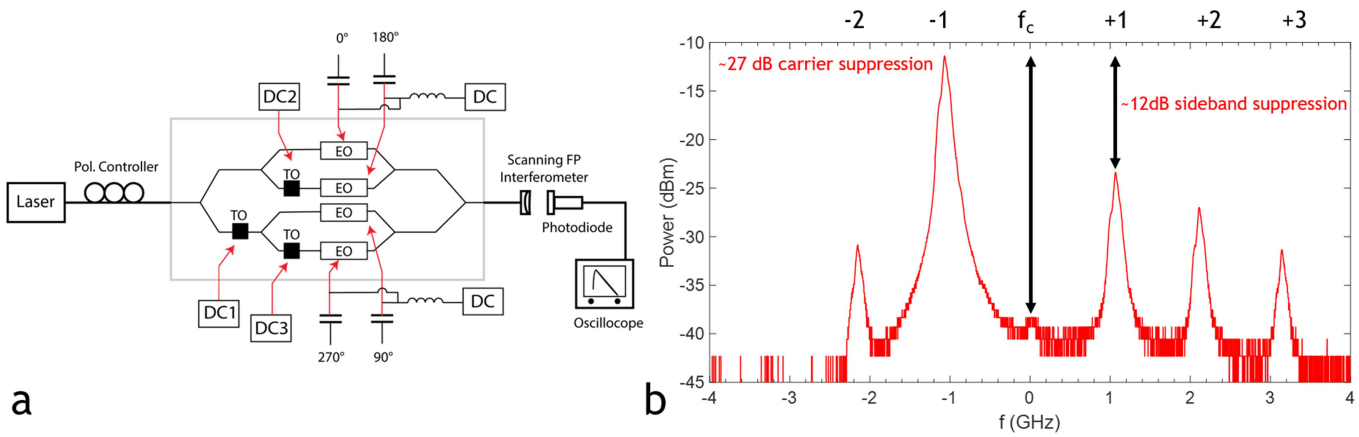

Fig. 2. (a) Experimental setup of an optical single-sideband modulator with an input laser at 1550 nm, polarization controller, and a scanning Fabry-Perot (FP) interferometer to an oscilloscope. DC and RF control lines for both TO phase shifters and EO modulators are in red. (b) SSB spectra with 1 GHz modulation and all controls optimized for the -1 sideband with carrier suppression greater than 25dB and an unwanted sideband suppression of 12dB. Total input RF and laser powers are +20dBm (i.e. 14dBm per modulator) and +13dBm respectively.

interferometer. We observe good performance with carrier suppression of 27 dB and sideband suppression of 12 dB with respect to the -1 sideband (see Figure 2b). Due to optical and electrical imbalances, we also see undesired spurious components in the form of +1, +2, and -2 sidebands. Of the initial +13dBm of the carrier, +3dBm remains accounting for ~10 dB insertion loss to and from the chip. If operated at the optimal RF power, the device has an intrinsic conversion loss from carrier to first sideband that's theoretically limited to -4.7 dB [2-3]. That's an expected first sideband power close to -2 dBm but we measure closer to -10 dBm. This difference can be attributed to off-optimal RF power operation, 2-3dB of absorption in the modulator and residual power in the spurious sidebands. Furthermore, we have characterized the performance of our SSB modulator as a function of input RF power and input laser power (see Figure 3a-b).

Additionally, not shown here, we have improved the sideband suppression to 17.5 dB with the use of ring filters on the output. Moreover, with the use of additional TO splitters that compensate for amplitude and phase imbalances all unwanted sidebands were reduced to below the detection limit without the use of any ring filters, but with increased insertion loss (see Figure 3c). Here, the upper and lower MZIs were optimized for maximum carrier suppression with an individual extinction of at least 50 dB [5-6].

Currently, we are actively pursuing active feedback mechanisms to improve the performance of the SSB modulator and make robust to perturbations over extended periods of time. Starting with a single MZI arm, we make use of high-contrast TO phase splitter (V_1 & V_2) to actively maintain an optimal output for maximum carrier suppression of SSB device. Figure 4a is the output spectra as a function of TO phase shifters V_1 & V_2 with a superimposed gradient map. We use the local gradient to locate and maintain optimal operating point for the MZI. With an initial setpoint (V_1,V_2 = 4,3 V), the output power converges within a minute and continues to operate at optimum with the presence of a temperature ramp on the sample stage.

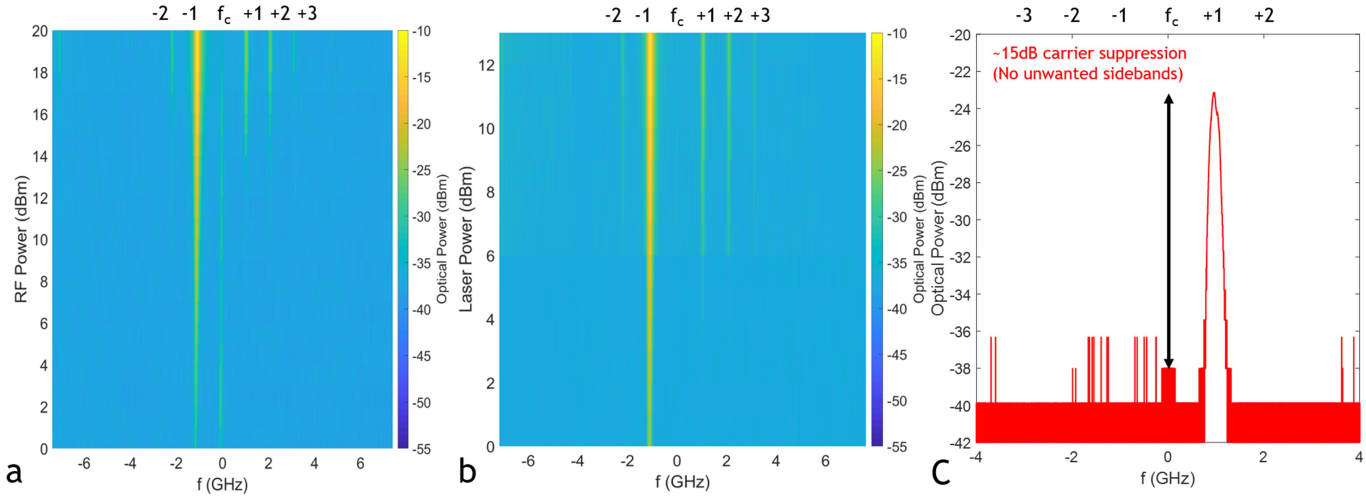

Fig. 3. (a) SSB spectra as a function of input RF power for a fixed laser power of +13 dBm. For low RF powers, there is observable decrease in carrier suppression. (b) Spectra as a function of input laser power at 1550nm for a fixed RF power of +20dBm. There is no noticeable effect on device performance. (c) SSB spectra showing no unwanted sidebands with the use of additional TO splitters to compensate for amplitude and phase imbalances operating at 1 GHz modulation with ~15dB carrier suppression.

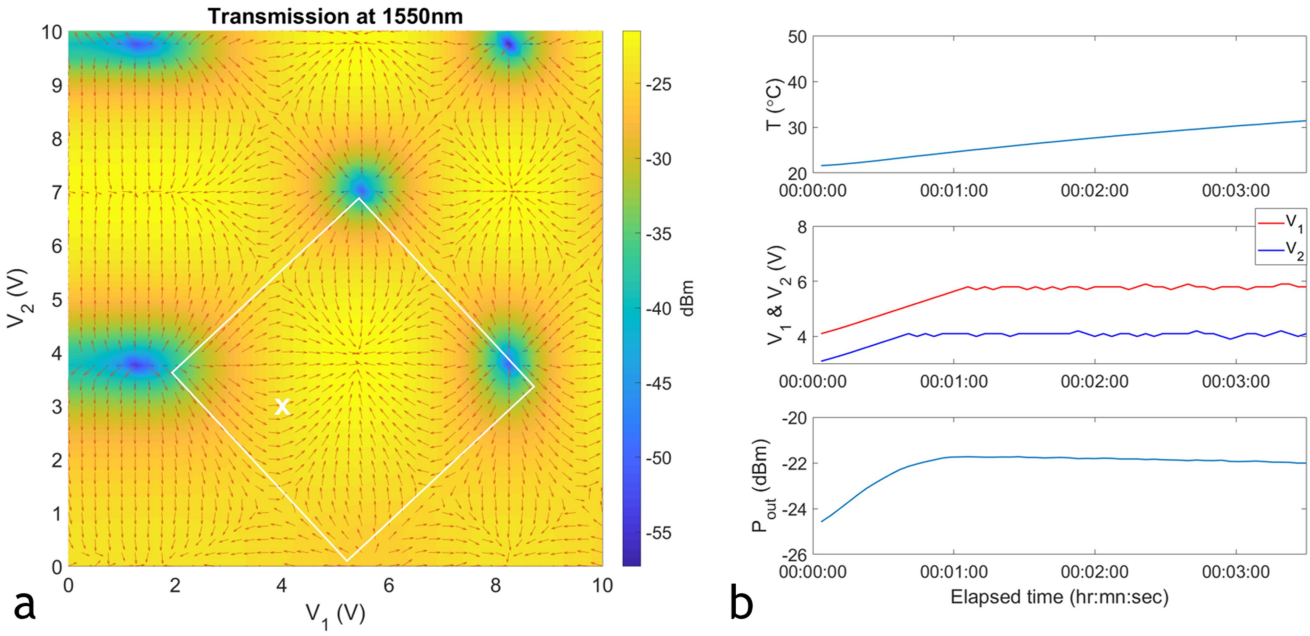

Fig. 4. (a) Output transmission spectra of a single MZI arm with the help of high-contrast TO phase splitter (V_1 & V_2) for maximum carrier suppression. The red arrows portray the gradient map. The white square is representative of the region of convergence for maximal output and 'x' marks the initial setpoint for feedback. (b) Time evolution of output power with an initial setpoint (V_1, V_2= 4, 3 V) following the local gradient with a simultaneous temperature ramp of the sample stage. As seen, the output power converges within a minute and continues to operate at maximal output power even as the temperature varies.

IV. Conclusion

We have demonstrated the first optical SSB modulator based on dual-parallel MZMs on a silicon platform with high carrier (27 dB) and sideband (12 dB) suppressions. With the use of additional TO elements compensating for phase and amplitude imbalances, all unwanted sidebands were drastically reduced. This device should be operational to the full bandwidth of the modulators (~7 GHz) and can go beyond 20 GHz with further refinement using travelling wave electrodes [7]. Furthermore, we plan to improve the performance and robustness of this device by implementing an active feedback mechanism for the whole SSB that compensates, in real-time, for the optical phase and amplitude imbalances present in the system. In comparison to other SSB modulators on silicon, this modulator is more efficient and suitable for high-power applications.

Acknowledgment

This work is supported by the Laboratory Directed Research and Development program at Sandia National Laboratories, a multi-mission laboratory managed and operated by National Technology & Engineering Solutions of Sandia, LLC, a wholly owned subsidiary of Honeywell International Inc., for the U.S. Department of Energy's National Nuclear Security Administration under contract DE-NA0003525. This paper describes technical results and analysis. Any subjective views or opinions that might be expressed in the paper do not necessarily represent the view of the U.S. Department of Energy or the United States Government.

References

[1] L. T. Nichols and R. D. Esman, "Single sideband modulation techniques and applications," OFC/IOOC **3**, 332 (1999).

[2] M. Izutsu *et al.*, "Integrated Optical SSB Modulator/Frequency Shifter," IEEE J. Quantum Electron. **17,** 11 (1981).

[3] S. Shimotsu *et al.*, "Single Side-Band Modulation Performance of a LiNbO3 Integrated Modulator Consisting of Four-Phase Modulator Waveguides," IEEE Photon. Technol. Lett. **13**, 4 (2001).

[4] B-M. Yu *et al.*, "Single-chip Si Optical single-sideband modulator," Photon. Res. **6**, 1 (2018).

[5] S. Liu *et al.*, "High speed ultra-broadband amplitude modulators with ultrahigh extinction >65dB," Opt. Express **25**, 10 (2017).

[6] Y. Ogiso *et al.*, "High Extinction-Ratio Integrated Mach-Zhender Modulator with Active Y-Branch for Optical SSB Signal Generation," IEEE Photon. Technol. Lett. **22**, 12 (2010).

[7] C. T. DeRose *et al.*, "High speed travelling wave carrier depletion silicon mach-zehnder modulator," Opt. Interconnects Conf., p135-36 (2012).